

# ACCURACY-ROBUSTNESS TRADE OFF VIA SPIKING NEURAL NETWORK GRADIENT SPARSITY TRAIL

**Nhan T. Luu**

College of Information and Communication Technology  
Can Tho University  
Can Tho, Vietnam

## ABSTRACT

Spiking Neural Networks (SNNs) have attracted growing interest in both computational neuroscience and artificial intelligence, primarily due to their inherent energy efficiency and compact memory footprint. However, achieving adversarial robustness in SNNs—particularly for vision-related tasks—remains a nascent and underexplored challenge. Recent studies have proposed leveraging sparse gradients as a form of regularization to enhance robustness against adversarial perturbations. In this work, we present a surprising finding: under specific architectural configurations, SNNs exhibit natural gradient sparsity and can achieve state-of-the-art adversarial defense performance without the need for any explicit regularization. Further analysis reveals a trade-off between robustness and generalization: while sparse gradients contribute to improved adversarial resilience, they can impair the model’s ability to generalize; conversely, denser gradients support better generalization but increase vulnerability to attacks.

## 1 INTRODUCTION

Recent decades have witnessed remarkable progress in the domain of artificial intelligence (AI), primarily fueled by the evolution of deep learning techniques (Wani et al., 2020). Nevertheless, conventional artificial neural networks (ANNs) often struggle to accurately replicate the complex and dynamic characteristics inherent in biological neural systems (Nguyen et al., 2021). In response to this limitation, spiking neural networks (SNNs) have gained attention as a biologically inspired alternative, exploiting the temporal dynamics of neuronal signaling to better reflect the functioning of the human brain.

SNNs communicate using discrete spike events, emulating the asynchronous and event-driven nature of biological neural communication (Auge et al., 2021). This spike-based mechanism not only improves the biological realism of computational models but also introduces benefits such as enhanced energy efficiency and suitability for neuromorphic hardware implementations (Blouw et al., 2019). The sparsity and temporally precise signaling intrinsic to SNNs make them ideal candidates for designing power-efficient systems capable of real-time processing (Rajendran et al., 2019).

Despite their advantages, SNNs present notable difficulties, particularly in terms of training and optimization. The non-differentiable nature of spike-based activity renders traditional backpropagation techniques unsuitable (Nunes et al., 2022). To overcome these obstacles, researchers have proposed alternative training paradigms, including spike-timing-dependent plasticity (STDP) (Srinivasan et al., 2017; Liu et al., 2021) and surrogate gradient methods (Neftci et al., 2019; Eshraghian et al., 2023; Fang et al., 2021a), which facilitate the learning process in spiking networks.

Robustness is critical in safety-sensitive domains like autonomous driving, where adversarial attacks—small, human-imperceptible input perturbations—can cause high-confidence misclassifications (Szegedy et al., 2013; Goodfellow et al., 2014). Despite advancements in defensive strategies, models remain vulnerable across architectures—even when trained for the same task (Madry et al., 2017). SNNs differ from ANNs in their spike-based, discrete-time signaling, prompting new considerations for adversarial vulnerability (Sharmin et al., 2020).

In this study, we investigate the role of gradient sparsity in SNNs and its impact on adversarial robustness and generalization. Through comprehensive empirical analysis, we find that under specific architectural configurations, SNNs exhibit naturally sparse input gradients. This inherent sparsity significantly impairs the effectiveness of white-box adversarial attacks (Ding et al., 2022), enabling the model to achieve state-of-the-art (SOTA) adversarial robustness without the use of any explicit regularization or defense mechanisms. However, this robustness comes at the cost of reduced undefended accuracy. Conversely, deliberately increasing gradient density leads to improved clean generalization but compromises robustness against adversarial perturbations. These findings suggest a fundamental trade-off between robustness and generalization in SNNs, governed by the degree of gradient sparsity. To the best of our knowledge, this is the first work to systematically uncover and characterize this duality. Our main contributions are as follows:

- We provide both theoretical analysis and empirical evidence demonstrating how natural gradient sparsity in SNNs contributes to adversarial robustness, and elucidate the underlying mechanisms driving this behavior.
- We theoretically and empirically characterize the robustness–generalization trade-off by manipulating the gradient sparsity through architectural and training configurations.

## 2 RELATED WORKS

### 2.1 SPIKING NEURAL NETWORKS

SNNs represent a biologically inspired extension of traditional ANNs, offering a fundamentally distinct computational framework. In contrast to ANNs, which utilize continuous-valued activations and gradient-based learning algorithms such as backpropagation (Rumelhart et al., 1986; Shrestha & Orchard, 2018), SNNs encode and transmit information through discrete spike events (Maass, 1997). This event-driven mechanism supports sparse and energy-efficient computation, making SNNs particularly well-suited for deployment on neuromorphic hardware (Merolla et al., 2014). While most conventional ANN architectures operate on dense, floating-point representations, SNNs emulate the asynchronous and temporally precise signaling of biological neurons (Gerstner & Kistler, 2002). Additionally, SNNs inherently process temporal data and can leverage learning rules like STDP for unsupervised training (Lee et al., 2018). However, the discontinuous nature of spikes presents significant challenges for optimization, often requiring alternative training strategies such as surrogate gradient methods (Neftci et al., 2019) or indirect approaches like ANN-to-SNN conversion (Rueckauer et al., 2017). As a result, SNNs offer a promising direction for energy-efficient and biologically plausible computation, while also posing distinct challenges in terms of training and network design.

Various surrogate gradient functions have been proposed (Fang et al., 2023; 2021a; Zenke & Ganguli, 2018; Esser et al., 2015; Zenke & Vogels, 2021), each with different trade-offs in terms of biological fidelity, computational efficiency, and training stability. These approximations enable effective error propagation through spiking layers, making it possible to train deep SNN architectures for complex image processing tasks (Fang et al., 2021a; Lee et al., 2020; Shrestha & Orchard, 2018). Together, these developments have contributed to bridging the performance gap between SNNs and their ANN counterparts, while maintaining the unique advantages of spiking computation.

### 2.2 ADVERSARIAL ROBUSTNESS IN LEARNING MODELS

Deep neural networks (DNNs) can be easily deceived into producing incorrect outputs on inputs that have been subtly altered in ways imperceptible to humans (Szegedy et al., 2013). While many adversarial-example generation methods (usually referred to as “adversarial attacks”) rely on white-box access to model parameters, recent work has demonstrated that even black-box models can be compromised in practice—largely owing to the transferability property of adversarial examples, whereby inputs crafted to mislead one model often generalize to other models trained on the same data (Papernot et al., 2017). In the context of image recognition, adversarial perturbations can be crafted to remain effective across different scales and viewing angles (Athalye et al., 2018b), posing a significant challenge to deploying deep learning in safety-critical applications such as autonomous vehicles.

Despite a surge of research into adversarial defenses, many proposed methods fail to withstand transferred attacks (Tramèr et al., 2017b). For instance, “feature squeezing” (Xu et al., 2017) sidesteps robust classification by simply detecting and discarding suspected adversarial inputs rather than correctly classifying them. The most straightforward defense—adversarial training—augments the training set with a mixture of clean and adversarially-perturbed examples (Kurakin et al., 2016). However, Tramèr et al. (2017a) showed that adversarial training can be undermined by randomizing perturbations or borrowing perturbations generated from different models, although employing model ensembles offers some mitigation.

Beyond robustness, practitioners are often troubled by the opacity of DNN predictions. This lack of interpretability is especially problematic in domains prone to algorithmic bias (Flores et al., 2016) or in medical settings where discrepancies between training and deployment contexts can introduce safety hazards Caruana et al. (2015). To address this, many methods aim to explain individual DNN decisions via interpretable local surrogate models—commonly linear approximations that capture the network’s behavior under small input perturbations (Ribeiro et al., 2016). A straightforward choice is to use the model’s input gradient, which provides a first-order Taylor approximation of how outputs change in response to input variations (Baehrens et al., 2010). However, for image classification, raw input gradients are often noisy and difficult to interpret. Consequently, techniques such as Integrated Gradients (Sundararajan et al., 2016) and SmoothGrad (Smilkov et al., 2017) have been developed to produce smoother, more visually coherent saliency maps by aggregating gradient information across multiple perturbed copies of the input.

### 3 ADVERSARIAL ATTACKS

In this section, we establish the notation used throughout while briefly outline the standard adversarial attack mechanisms that serve as baselines for comparison, which applies to any differentiable classifier denoted by  $f_\theta(X)$ , where  $\theta$  represents the model parameters. The model produces prediction outputs  $\hat{y} \in \mathbb{R}^{N \times K}$  for input data  $X \in \mathbb{R}^{N \times D}$ , with  $N$  samples of dimensionality  $D$ , each classified into one of  $K$  categories. These predictions correspond to class probabilities for each input instance.

Training such models involves optimizing the parameter set  $\theta^*$  to minimize the divergence between the predicted outputs  $\hat{y}$  and the ground truth labels  $y \in \mathbb{R}^{N \times K}$  (represented in one-hot encoding). This is typically achieved by minimizing the overall cross-entropy loss (Ross & Doshi-Velez, 2018):

$$\begin{aligned} \theta^* &= \arg \min_{\theta} \sum_{n=1}^N \sum_{k=1}^K -y_{nk} \log f_\theta(X_n)_k \\ &= \arg \min_{\theta} H(y, \hat{y}) \end{aligned} \tag{1}$$

where  $H$  denotes the total cross-entropy between the true and predicted distributions.

#### 3.1 FAST GRADIENT SIGN METHOD (FGSM)

Introduced by Goodfellow et al. (2014), this approach perturbs input samples in the direction of the gradient sign of the loss with respect to the inputs. The perturbed adversarial examples are given by:

$$X_{\text{FGSM}} = X + \epsilon \cdot \text{sign}(\nabla_x H(y, \hat{y})), \tag{2}$$

where  $\epsilon$  controls the magnitude of the perturbation. Although small in scale, these modifications can substantially degrade model performance while remaining imperceptible to human observers. Kurakin et al. (2018) extended this method by applying it multiple times with smaller step sizes. This iterative variant follows the gradient path more accurately, resulting in stronger adversarial examples that require less overall distortion.

#### 3.2 PROJECTED GRADIENT DESCENT (PGD)

Building upon the FGSM framework, the PGD attack (introduced by Madry et al. (2017)) is considered one of the most potent first-order adversaries. It generates adversarial examples by iteratively applying small perturbations in the direction of the gradient sign of the loss with respect to the input,

while projecting the perturbed input back onto the  $\ell_\infty$  ball of radius  $\epsilon$  centered around the original input. Formally, each update step is given by:

$$X^{t+1} = \Pi_{\mathcal{B}_\epsilon(X)}(X^t + \alpha \cdot \text{sign}(\nabla_x H(y, \hat{y}))), \quad (3)$$

where  $\Pi_{\mathcal{B}_\epsilon(X)}(\cdot)$  denotes the projection operator onto the  $\ell_\infty$  ball  $\mathcal{B}_\epsilon(X)$ ,  $\alpha$  is the step size, and  $t$  is the iteration index. By repeating this process for multiple steps, PGD generates adversarial examples that are more effective at deceiving neural networks, while still remaining within the specified perturbation bound. This iterative process significantly enhances attack strength compared to single-step methods like FGSM.

## 4 EVALUATION AND ANALYSIS

### 4.1 OVERALL SETTINGS

For undefended benchmarking, we employed SEW-ResNet (Fang et al., 2021a) and Spiking-ResNet (Hu et al., 2021) variants. Model implementation and experimental procedures leveraged PyTorch (Paszke et al., 2019) and SpikingJelly (Fang et al., 2023).

For preprocessing, we performed image normalization within the range of [0, 1] and horizontal random flip during training as augmentation method (Wang et al., 2017) for better generalization. Optimization was facilitated by applying Backward Pass Through Time (BPTT) (Ding et al., 2022; Fang et al., 2021b) with surrogate gradient (Fang et al., 2021a) to all Integrate-and-Fire (IF) neurons, utilizing the arctan surrogate function (Fang et al., 2021a; Eshraghian et al., 2023). Its derivative,  $\partial\mathcal{H}/\partial x$ , for the Heaviside function  $\mathcal{H}(x, V_{th})$  with potential voltage  $V_{th}$  and input  $x$  during back-propagation is defined as:

$$\begin{aligned} \mathcal{H}(x, V_{th}) &= \begin{cases} 1 & \text{if } x - V_{th} \geq 0 \\ 0 & \text{otherwise} \end{cases} \\ \frac{\partial\mathcal{H}}{\partial x} &= \frac{\alpha}{2 \left(1 + \left(\frac{\pi}{2}\alpha x\right)^2\right)} \quad \text{where } \alpha = 2 \end{aligned} \quad (4)$$

For spike encoding, we adopted the well-established *phase coding* (Kim et al., 2018) with a time step size of  $T = 10$ , spike weight  $\omega(t)$  where  $t \in T$  is given by:

$$\omega(t) = 2^{-(1+\text{mod}(t-1, K))}.$$

Consistent with prior work in ANN and SNN optimization (Luu et al., 2023; 2024a;b;c), cross-entropy loss (mentioned in Equation 1) along with the Adam algorithm (Kingma & Ba, 2014) was used for optimization. A learning rate of  $lr = 1 \times 10^{-3}$  and parameters  $\beta = (0.9, 0.999)$  were applied for optimizer across all evaluated datasets. All training was conducted with a batch size of 16 images for 100 epochs on an NVIDIA RTX 3090 GPU. We also use deterministic random seeding (Picard, 2021) to ensure reproducibility and avoid stochastic gradient problem (Athalye et al., 2018a). To evaluate the comparative performance of our model in image classification tasks, we utilize *Accuracy*—a widely adopted metric that quantifies how well a model predicts the correct labels. Specifically, accuracy represents the ratio of correctly predicted labels  $\hat{y}_i$  matching the true labels  $y_i$  across a dataset of  $N$  instances, and is formally defined as:

$$\text{Accuracy} = \frac{1}{N} \sum_{i=1}^N \mathbb{1}(\hat{y}_i = y_i)$$

Here,  $\mathbb{1}(\cdot)$  denotes the indicator function, which yields 1 if the argument is true and 0 otherwise.

### 4.2 NATURAL ADVERSARIAL ROBUSTNESS OF SNN

We benchmark our selected models against several SOTA methods aimed at enhancing the adversarial robustness of spiking neural networks. Specifically, we compare our undefended SNN variants with input discretization (Sharmin et al., 2020), Hire-SNN (Kundu et al., 2021), and SNN-RAT

Table 1: Comparison of CIFAR-100 (Alex, 2009) validation accuracy of undefended SNN variants with various SNN adversarial defense methods. Best performance per attack are denoted in bold. The upper section showcases the accuracy of existing SOTA defend methods, while the lower section details the performance of undefended SEW-ResNet and Spiking-ResNet variants. Notably, undefended SEW-ResNet achieve SOTA performance against PGD attacks and reasonable performance against FGSM attacks.

| SNN variants                                | Validation accuracy per attack (%) |              |              |
|---|------------------------------------|--------------|--------------|
|   | FGSM                               | PGD          | Clean        |
| Input discretization (Sharmin et al., 2020) | 15.50                              | 6.30         | 64.40        |
| Hire-SNN (Kundu et al., 2021)               | 22.00                              | 7.50         | 65.10        |
| Vanilla VGG-11 (Ding et al., 2022)          | 5.30                               | 0.02         | <b>73.33</b> |
| SNN-RAT VGG-11 (Ding et al., 2022)          | 25.86                              | 10.38        | 70.89        |
| SNN-RAT WRN-16 (Ding et al., 2022)          | <b>28.08</b>                       | 11.31        | 69.32        |
| SEW-ResNet18 (Fang et al., 2021a)           | 20.81                              | 13.47        | 42.19        |
| SEW-ResNet34 (Fang et al., 2021a)           | 19.91                              | 13.25        | 41.81        |
| SEW-ResNet50 (Fang et al., 2021a)           | 21.27                              | <b>16.03</b> | 38.91        |
| Spiking-ResNet18 (Hu et al., 2021)          | 13.36                              | 11.15        | 23.23        |
| Spiking-ResNet34 (Hu et al., 2021)          | 2.43                               | 1.64         | 21.20        |
| Spiking-ResNet50 (Hu et al., 2021)          | 3.32                               | 2.44         | 20.56        |

Table 2: Comparison of validation accuracy of undefended SEW-ResNet variants with various SNN adversarial defense methods on multiple vision datasets. Best performance per attack on each dataset are denoted in bold. Results are consistent even with different datasets.

| Datasets  | SNN variants                       | Validation accuracy per attack (%) |              |              |
|-----------|------------------------------------|------------------------------------|--------------|--------------|
|           |                                    | FGSM                               | PGD          | Clean        |
| CIFAR-10  | SNN-RAT VGG-11 (Ding et al., 2022) | 45.23                              | 21.16        | 90.74        |
|           | SNN-RAT WRN-16 (Ding et al., 2022) | 50.78                              | 22.71        | <b>92.69</b> |
|           | SEW-ResNet18 (Fang et al., 2021a)  | 46.99                              | 34.33        | 73.78        |
|           | SEW-ResNet34 (Fang et al., 2021a)  | 49.20                              | 36.98        | 74.16        |
|           | SEW-ResNet50 (Fang et al., 2021a)  | <b>51.09</b>                       | <b>40.55</b> | 73.34        |
| CIFAR-100 | SNN-RAT VGG-11 (Ding et al., 2022) | 25.86                              | 10.38        | <b>70.89</b> |
|           | SNN-RAT WRN-16 (Ding et al., 2022) | <b>28.08</b>                       | 11.31        | 69.32        |
|           | SEW-ResNet18 (Fang et al., 2021a)  | 20.81                              | 13.47        | 42.19        |
|           | SEW-ResNet34 (Fang et al., 2021a)  | 19.91                              | 13.25        | 41.81        |
|           | SEW-ResNet50 (Fang et al., 2021a)  | 21.27                              | <b>16.03</b> | 38.91        |

(Ding et al., 2022), all of which have demonstrated notable improvements under adversarial settings. The evaluations will focus on standard attack methods such as FGSM and PGD and all models will be benchmarked using fixed settings for adversarial attacks. Specifically,  $\epsilon = 8/255$  will be used for both FGSM and PGD, with PGD further configured with  $\alpha = 0.01$  and  $t = 7$ , consistent with previous researches (Ding et al., 2022).

As presented in Table 1, all SEW-ResNet variants exhibit SOTA performance against PGD attacks, achieving up to 16.03% accuracy—an improvement of 4.72% over the previous best method (SNN-RAT WRN-16). For FGSM attacks, SEW-ResNet50 yields a competitive 21.27% accuracy, which is only 4.59% below SNN-RAT and nearly equivalent to the performance of Hire-SNN, leading us to suspect that the benchmarking result was affected by obfuscated gradient Athalye et al. (2018a). In contrast, Spiking-ResNet variants without any defense mechanism do not exhibit similar resilience as deeper residual blocks being constructed, therefore we would only continue benchmarking with SEW-ResNet variants. From Table 2, we can see that this behavior not only consistent on multiple dataset, SEW-ResNet50 was able to outperform all mentioned adversarial defense mechanism with a 0.31% gap on FGSM and 17.84% gap on PGD (compare with SNN-RAT WRN-16).

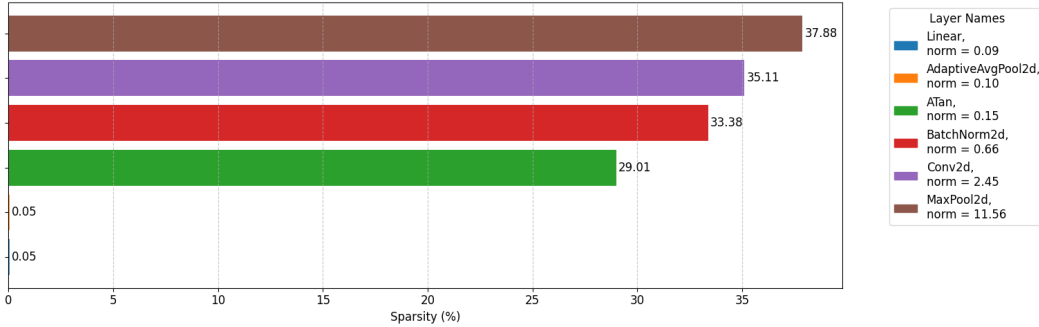


Figure 1: Inspection of average input gradient sparsity and input gradient norm across all employed operations within SEW-ResNet18. Gradient was clearly defined and high sparsity mostly occurs in operations of SEW residual blocks.

#### 4.3 EXPLANATION AND ANALYSIS

As demonstrated in the benchmarking results presented in Section 4.2, we observe that undefended SEW-ResNet exhibit a notable degree of adversarial robustness, achieving performance comparable to SOTA defense methods but Spiking-ResNet does not exhibit the same behavior. This raises a fundamental question: *Why do SNNs demonstrate such inherent robustness in the absence of explicit defense mechanisms?*

We hypothesize that this phenomenon arises from the inherent sparsity of input gradients in SEW-ResNet, which in turn reduces the efficacy of adversarial perturbations. Supporting this hypothesis, prior work (Liu et al., 2024) has shown that SNNs show strong resistance against random perturbation at significant scale, where the distance between random vulnerability and adversarial vulnerability can be upper bounded by the sparsity of the input gradient as:

**Theorem 1** (Liu et al.). *Suppose  $f$  is a differentiable SNN by surrogate gradients, and  $\epsilon$  is the magnitude of an attack, assumed to be small enough. Given an input image  $\mathbf{x}$  with corresponding label  $y$ , the ratio of  $\rho_{adv}(f, \mathbf{x}, \epsilon, \ell_\infty)$  and  $\rho_{rand}(f, \mathbf{x}, \epsilon, \ell_\infty)$  is upper bounded by the sparsity of  $\nabla_{\mathbf{x}} f_y$ :*

$$3 \leq \frac{\rho_{adv}(f, \mathbf{x}, \epsilon, \ell_\infty)}{\rho_{rand}(f, \mathbf{x}, \epsilon, \ell_\infty)} \leq 3 \|\nabla_{\mathbf{x}} f_y(\mathbf{x})\|_0.$$

As observed from the theorem, adversarial vulnerability  $\rho_{adv}(f, \mathbf{x}, \epsilon, \ell_\infty)$  scale positively with non-zero entries in input gradient, we can form a corollary as:

**Corollary 1.** *The adversarial vulnerability  $\rho_{adv}(f, \mathbf{x}, \epsilon, \ell_\infty)$  scale positively with non-zero entries of input gradient  $\|\nabla_{\mathbf{x}} f_y(\mathbf{x})\|_0$ .*

To validate this explanation in light of the theorem, we conduct an empirical analysis of the input gradient patterns for SEW-ResNet models under adversarial perturbations. Specifically, we compute the average percentage of non-zero entries in the input gradients (as shown in Figure 1). Additionally, we measure the gradient norm to ensure that the sparsity is not a byproduct of shattered gradients, following the recommendations from Athalye et al. (2018a).

While gradient was clearly defined as norm was calculable, gradient sparsity emerges predominantly within residual blocks from 29.01% in IF neurons surrogate gradient to 37.88% in max pooling gradient, particularly in components such as convolutional layers, batch normalization, max pooling, and arctan surrogate gradients of IF neurons. This sparsity may serve as a natural regularization mechanism, assisting in gradient-based attacks mitigation and contributing to the enhanced robustness observed in our experiments.

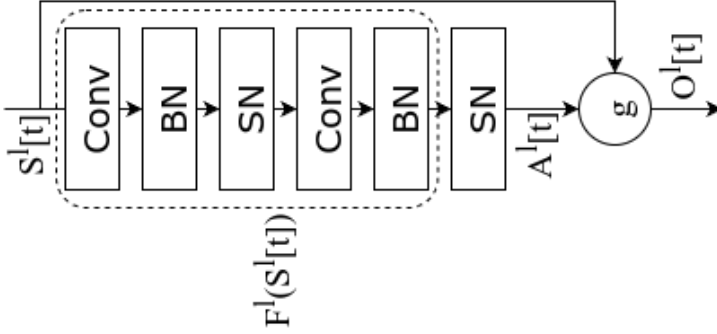


Figure 2: Architecture of SEW residual block proposed by Fang et al. (2021a)

$$\begin{aligned}
\frac{\partial \text{Conv}(x, \mathbf{w})}{\partial x} &= \text{Conv}^\top \left( \frac{\partial \mathcal{L}}{\partial y}, \mathbf{w} \right), \\
\frac{\partial \text{BN}(y_{i,c})}{\partial x_{i,c}} &= \frac{\gamma_c}{\sqrt{\sigma_c^2 + \varepsilon}} \left[ \delta_{i,c} - \sum_j^m \frac{\delta_{j,c}}{m} - \frac{\hat{x}_{i,c}}{m} \sum_j^m \delta_{j,c} \cdot \hat{x}_{j,c} \right], \\
\delta_{i,c} &= \frac{\partial \mathcal{L}}{\partial y_{i,c}} \\
\hat{x}_{i,c} &= \frac{x_{i,c} - \mu_c}{\sqrt{\sigma_c^2 + \varepsilon}}, \quad y_{i,c} = \gamma_c \hat{x}_{i,c} + \beta_c \\
\mu_c &= \frac{1}{m} \sum_{i=1}^m x_{i,c}, \quad \sigma_c^2 = \frac{1}{m} \sum_{i=1}^m (x_{i,c} - \mu_c)^2 \\
\frac{\partial \text{MaxPool}(x)}{\partial x_{i,j}} &= \begin{cases} \frac{\partial \mathcal{L}}{\partial y_{p,q}} & \text{if } x_{i,j} = \max_{(m,n) \in \mathcal{R}_{p,q}} x_{m,n} \\ 0 & \text{otherwise} \end{cases} \\
\frac{\partial \mathcal{H}}{\partial x} &= \frac{\alpha}{2 \left( 1 + \left( \frac{\pi}{2} \alpha x \right)^2 \right)} \quad \text{where } \alpha = 2
\end{aligned} \tag{5}$$

Upon further analysis, we identified two distinct types of gradient sparsity emerging from these operations, which we categorize as:

- *Architectural sparsity* where input gradient sparsity occurred mostly due to intentional architectural choice.
- *Natural sparsity* where input gradient sparsity occurred due to the nature of spike signal instead of model design influence.

To quantify these sources, we analyze the gradient expressions of each component within the spike-based element-wise residual blocks. In Equation 5,  $\text{Conv}$  and  $\text{Conv}^\top$  refer to the forward and transposed convolution operations respectively.  $\mathcal{L}$  denotes the loss function,  $\mathbf{w}$  the kernel weights, and  $y$  the output of the operation. For the batch normalization (BN) gradient,  $\gamma_c$  and  $\beta_c$  represent the learned scale and shift parameters for channel  $c$ , while  $\mu_c$  and  $\sigma_c^2$  are the mean and variance computed across the batch of size  $m$ . The notation  $\hat{x}_{i,c}$  is the normalized input, and  $\delta_{i,c}$  represents the partial derivative of the loss with respect to the BN output. The max pooling gradient selectively propagates gradients only through the maximum element within each pooling region  $\mathcal{R}_{p,q}$ , and  $\mathcal{H}$  denotes the arctangent surrogate gradient of IF neurons, controlled by the slope parameter  $\alpha$ .

As seen in Equation 5, convolution, batch normalization, and surrogate gradient components are all dependent on input and intermediate values. However, max pooling introduces a structural bottleneck where gradients are non-zero only at the maximum activation locations, and zero elsewhere. These null gradients can propagate through backward pass, create sparsity in earlier layers and is

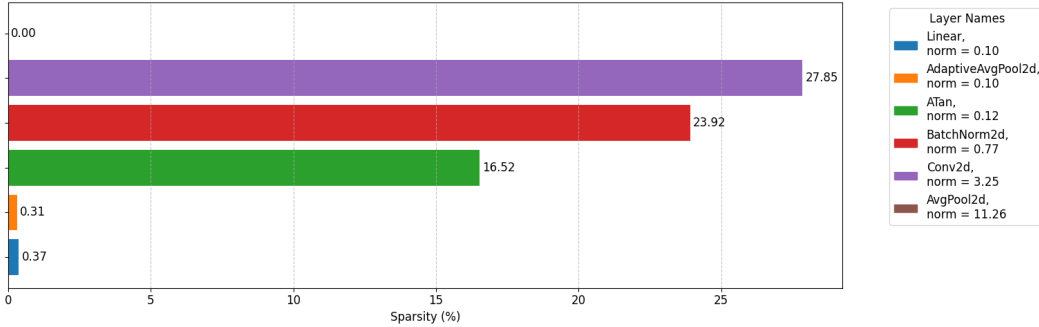


Figure 3: Inspection of average input gradient sparsity and input gradient norm across all employed operations within SEW-ResNet18 when employed with average pooling. Sparsity significantly reduced when compared with result in Figure 1.

Table 3: Comparison of CIFAR-100 and CIFAR-10 validation accuracy of undefended SEW-ResNet variants (Fang et al., 2021a) with average pooling. Best performance per attack on each dataset are denoted in bold. We employed similar attack settings as Table 1, accuracy reduction with respect to Table 2 is denoted in red and accuracy increment is denoted in green. There is a clear trade off in clean accuracy and adversarial robustness.

| Datasets  | SNN variants | Validation accuracy per attack (%) |                               |                               |
|-----------|--------------|------------------------------------|-------------------------------|-------------------------------|
|           |              | FGSM                               | PGD                           | Clean                         |
| CIFAR-10  | SEW-ResNet18 | 45.71 ( <b>↓1.28</b> )             | 25.72 ( <b>↓8.61</b> )        | 75.76 ( <b>↑1.98</b> )        |
|           | SEW-ResNet34 | 48.72 ( <b>↓0.48</b> )             | 29.82 ( <b>↓7.16</b> )        | <b>76.17</b> ( <b>↑2.01</b> ) |
|           | SEW-ResNet50 | <b>49.88</b> ( <b>↓1.21</b> )      | <b>33.29</b> ( <b>↓7.26</b> ) | 75.28 ( <b>↑1.94</b> )        |
| CIFAR-100 | SEW-ResNet18 | 17.93 ( <b>↓2.88</b> )             | 8.65 ( <b>↓4.82</b> )         | 43.32 ( <b>↑1.13</b> )        |
|           | SEW-ResNet34 | 20.07 ( <b>↓0.16</b> )             | 10.37 ( <b>↓2.88</b> )        | <b>44.58</b> ( <b>↑2.77</b> ) |
|           | SEW-ResNet50 | <b>22.02</b> ( <b>↓0.74</b> )      | <b>13.37</b> ( <b>↓2.66</b> ) | 43.40 ( <b>↑4.49</b> )        |

denoted as *architectural sparsity*. This effect is amplified in SEW-ResNet due to the high coupling nature of residual blocks (illustrated in Figure 2). Thus, replacing max pooling with a less sparse alternative could enhance gradient density. To evaluate this hypothesis, we replaced max pooling operations with average pooling, whose gradient is given by:

$$\frac{\partial \text{AvgPool}}{\partial x_{i,j}} = \sum_{(p,q) : (i,j) \in \mathcal{R}_{p,q}} \frac{1}{|\mathcal{R}_{p,q}|} \cdot \frac{\partial \mathcal{L}}{\partial y_{p,q}} \quad (6)$$

This formulation distributes gradients evenly across all elements in the receptive field  $\mathcal{R}_{p,q}$ , effectively reducing the degree of gradient sparsity, allow it to have broader impact during gradient-based optimization. We then re-evaluate SEW-ResNet variants’ performance under this setting and measure the resulting input gradient sparsity along with their adversarial robustness. The results are detailed in Figure 3 and Table 3.

From the results in Table 3, we observe that adversarial robustness of SEW-ResNet variants decrease when average pooling is employed in SEW-ResNet variants. Specifically, SEW-ResNet variants validation accuracy decrease under both FGSM and PGD attacks, with accuracy as low as 0.16% and 2.88% for SEW-ResNet34 on CIFAR-100 and as high as 1.28% and 8.61% for SEW-ResNet18 on CIFAR-10. Vice versa, models are able to improve generalization on clean validation, range from 1.13% (for SEW-ResNet18) to 4.49% (for SEW-ResNet50) on CIFAR-100.

As shown in Figure 3, input gradient sparsity is significantly reduced when average pooling is used in place of max pooling across all layers. Specifically, sparsity in the pooling layer is completely eliminated, leading to a 37.88% reduction compared to max pooling, while a spiking neuron layers exhibit sparsity as low as 16.52%. This observation is consistent with prior studies. For instance, Fang et al. (2021a) highlighted the importance of gradient magnitude in optimizing SNNs to enhance performance, while Luu et al. (2024b) addressed training challenges by introducing signal concate-

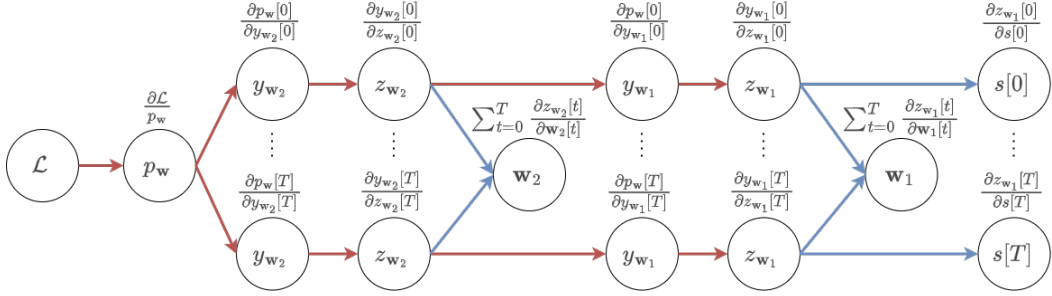


Figure 4: Backpropagation graph of Equation 7. Red arrow denoted shared gradient trails and blue denote variable specific gradient trail. Sparsity within shared gradient trail traverse to both input and optimizable parameters.

nation, effectively scaling the gradient norm to improve generalization. Complete elimination of sparsity is also theoretically unachievable due to the inherent nature of SNNs. This residual sparsity arises from the binary nature of the spiking function—typically modeled using the Heaviside function as in Equation 4—and is thus referred to as *natural sparsity*.

## 5 HOW DOES SHARED SPARSITY TRAIL IN GRADIENT COMPUTATION AFFECT PERFORMANCE?

Previous studies have demonstrated a strong relationship between the magnitude of weight gradients and model performance (Luu et al., 2024b; Fang et al., 2021a; Shalev-Shwartz et al., 2017). Building on this foundation, we aim to investigate how sparsity in the input gradients may suppress weight gradients during optimization, thereby influencing overall performance. To prove this statement, we consider the following theorem:

**Theorem 2.** *Given a multilayer SNN of the form:*

$$\begin{aligned} p_{\mathbf{w}}(s) &= \mathbb{E}_T [y_{w_2}(y_{w_1}(s[t]))] \quad \text{where } t \in T \\ y_{w_1}(\mathbf{x}) &= \Theta(z_{w_1}(\mathbf{x})), \quad z_{w_1}(\mathbf{x}) = \mathbf{w}_1 \cdot \mathbf{x} \\ y_{w_2}(\mathbf{x}) &= \Theta(z_{w_2}(\mathbf{x})), \quad z_{w_2}(\mathbf{x}) = \mathbf{w}_2 \cdot \mathbf{x} \end{aligned} \quad (7)$$

where  $s[t] \in \{0, 1\}^{T \times d}$  is the input signal,  $\mathbf{w}_l \in \mathbb{R}^{d \times d}$  are the model parameter matrices at layer  $l$  and  $\Theta(x, V_{th})$  is the hard-reset IF neurons with membrane potential  $V_{th}$ , defined as:

$$\begin{aligned} \Theta(s[t], V_{th}) &= \begin{cases} 1 & \text{if } s[t] - V_{th} \geq 0 \\ 0 & \text{otherwise} \end{cases} \\ \frac{\partial \Theta}{\partial s[t]} &= \frac{1}{1 + (\pi \cdot s[t])^2} \end{aligned} \quad (8)$$

Then as a result, we would have the following:

1. Any sparsity occur within the shared gradient chain will traverse back to both input gradient and weight gradient.
2. Parameters that are placed closer to the initial input signal will shared a longer gradient chain, making sparsity in input gradient have a stronger correlation with parameter gradient.

*Proof.* The input gradient  $\nabla_{s[t]} p_{\mathbf{w}}(s)$  of signal  $s[t]$  at timestep  $t$  can be quantified as:

$$\begin{aligned} \nabla_{s[t]} p_{\mathbf{w}}(s) &= \frac{\partial p_{\mathbf{w}}}{\partial y_{w_2}} \cdot \frac{\partial y_{w_2}}{\partial z_{w_2}} \cdot \frac{\partial z_{w_2}}{\partial y_{w_1}} \cdot \frac{\partial y_{w_1}}{\partial z_{w_1}} \cdot \frac{\partial z_{w_1}}{\partial s[t]} \\ &= \frac{1}{T} \cdot \frac{\mathbf{w}_2}{1 + (\pi \cdot \mathbf{w}_2 \cdot \Theta(\mathbf{w}_1 \cdot s[t]))^2} \cdot \frac{\mathbf{w}_1}{1 + (\pi \cdot \mathbf{w}_1 \cdot s[t])^2}, \end{aligned}$$

and the cumulative model Jacobian  $\nabla_{\mathbf{w}_l} p_{\mathbf{w}}(s)$  of  $\mathbf{w}_l$  at each layer  $l$  is:

$$\begin{aligned}\nabla_{\mathbf{w}_2} p_{\mathbf{w}}(s) &= \frac{\partial p_{\mathbf{w}}}{\partial y_{\mathbf{w}_2}} \cdot \frac{\partial y_{\mathbf{w}_2}}{\partial z_{\mathbf{w}_2}} \cdot \frac{\partial z_{\mathbf{w}_2}}{\partial \mathbf{w}_2} = \mathbb{E}_T \left[ \frac{\Theta(\mathbf{w}_1 \cdot s[t])}{1 + (\pi \cdot \mathbf{w}_2 \cdot \Theta(\mathbf{w}_1 \cdot s[t]))^2} \right] \\ \nabla_{\mathbf{w}_1} p_{\mathbf{w}}(s) &= \frac{\partial p_{\mathbf{w}}}{\partial y_{\mathbf{w}_2}} \cdot \frac{\partial y_{\mathbf{w}_2}}{\partial z_{\mathbf{w}_2}} \cdot \frac{\partial z_{\mathbf{w}_2}}{\partial y_{\mathbf{w}_1}} \cdot \frac{\partial y_{\mathbf{w}_1}}{\partial z_{\mathbf{w}_1}} \cdot \frac{\partial z_{\mathbf{w}_1}}{\partial \mathbf{w}_1} \\ &= \mathbb{E}_T \left[ \frac{\mathbf{w}_2}{1 + (\pi \cdot \mathbf{w}_2 \cdot \Theta(\mathbf{w}_1 \cdot s[t]))^2} \cdot \frac{s[t]}{1 + (\pi \cdot \mathbf{w}_1 \cdot s[t])^2} \right]\end{aligned}\quad (9)$$

As obtained from the derivation results, input gradient  $\nabla_{s[t]} p_{\mathbf{w}}(s)$  shared a gradient chain  $\frac{\partial p_{\mathbf{w}}}{\partial y_{\mathbf{w}_2}} \cdot \frac{\partial y_{\mathbf{w}_2}}{\partial z_{\mathbf{w}_2}} \cdot \frac{\partial z_{\mathbf{w}_2}}{\partial y_{\mathbf{w}_1}} \cdot \frac{\partial y_{\mathbf{w}_1}}{\partial z_{\mathbf{w}_1}}$  with the Jacobian  $\nabla_{\mathbf{w}_1} p_{\mathbf{w}}(s)$  of  $\mathbf{w}_1$  during backward computation and a shorter chain of  $\frac{\partial p_{\mathbf{w}}}{\partial y_{\mathbf{w}_2}} \cdot \frac{\partial y_{\mathbf{w}_2}}{\partial z_{\mathbf{w}_2}}$  with respect to  $\mathbf{w}_2$ , leading us to several observations:

- Any sparsity occur within the shared gradient chain will traverse back to both input gradient and weight gradient.
- Parameters that are placed closer to the initial input signal will shared a longer gradient chain, making sparsity in input gradient have a stronger correlation with parameter gradient<sup>1</sup>

□

We are confident that any sparsity in the shared gradient path propagates backward to both the weight and input gradients. Still, opposite of sparsity, how can we formally quantify the relationship between the density of the weight gradient (specifically of  $\mathbf{w}_1$ , as it is being the closest parameter to input and is highly affected by the shared gradient trail) with respect to input gradient, particularly in the context of Theorem 2? To address this, we establish the following theorem, which provides a precise characterization of their relationship:

**Theorem 3.** *Given the same condition as Theorem 2, the parameter matrix  $\mathbf{w}_l \in \mathbb{R}^{d_1 \times d_2}$  at layer  $l$  is said to have a row/column density degree of  $k_{\mathbf{w}_l}^{(i)}/k_{\mathbf{w}_l}^{(j)}$  (or  $k_{\mathbf{w}_l}^{(i)}/k_{\mathbf{w}_l}^{(j)}$ -dense row/column for short) if each of its row/column vector  $\mathbf{w}_l^{(i)}/\mathbf{w}_l^{(j)}$  (where  $i \in d_1$ ,  $j \in d_2$ ) has at most  $k$  non-zero entries  $\mathbf{w}_l^{(ij)}$ , defined as:*

$$\begin{aligned}k_{\mathbf{w}_l}^{(i)} &= \sup_{i \in d_1} \left( \#\{ \mathbf{w}_l^{(ij)} \in \mathbf{w}_l^{(i)} \mid \mathbf{w}_l^{(ij)} \neq 0 \} \right) = \sup_{i \in d_1} \left( \#\text{supp} \left( \mathbf{w}_l^{(i)} \right) \right) = \sup_{i \in d_1} \left( \|\mathbf{w}_l^{(i)}\|_0 \right), \\ k_{\mathbf{w}_l}^{(j)} &= \sup_{j \in d_2} \left( \#\{ \mathbf{w}_l^{(ij)} \in \mathbf{w}_l^{(j)} \mid \mathbf{w}_l^{(ij)} \neq 0 \} \right) = \sup_{j \in d_2} \left( \#\text{supp} \left( \mathbf{w}_l^{(j)} \right) \right) = \sup_{j \in d_2} \left( \|\mathbf{w}_l^{(j)}\|_0 \right),\end{aligned}\quad (10)$$

and for a vector  $\mathbf{v} \in \mathbb{R}^d$  as:

$$k_{\mathbf{v}} = \sup_{i \in d} \left( \#\{ \mathbf{v}^{(i)} \in \mathbf{v} \mid \mathbf{v}^{(i)} \neq 0 \} \right) = \sup_{i \in d} (\#\text{supp}(\mathbf{v})) = \sup_{i \in d} (\|\mathbf{v}\|_0). \quad (11)$$

If the  $L_0$  norm of input gradient and weight gradient can be defined as:

$$\begin{aligned}\|\nabla_{s[t]} p_{\mathbf{w}}(s)\|_0 &= \|\mathbf{w}_2 \cdot \mathbf{w}_1\|_0, \\ \|\nabla_{\mathbf{w}_1} p_{\mathbf{w}}(s)\|_0 &= \sum_{t=1}^T \|\mathbf{w}_2 \cdot s[t]\|_0 = \|\mathbf{w}_2 \cdot S\|_0 \quad (S \in \{0, 1\}^{d \times T}),\end{aligned}\quad (12)$$

then  $L_0$  norm of weight gradient of  $\mathbf{w}_1$  can bounded as:

$$\mathbb{E} [\|\nabla_{\mathbf{w}_1} p_{\mathbf{w}}(s)\|_0] \leq \frac{T}{d} \cdot \frac{k_S^{(j)}}{k_{\mathbf{w}_1}^{(j)}} \cdot \mathbb{E} [\|\nabla_{s[t]} p_{\mathbf{w}}(s)\|_0].$$

<sup>1</sup>A more illustrative demonstration can be found at Figure 4

*Proof.* Each entry in the input gradient is defined as:

$$\nabla_{s[t]} p_{\mathbf{w}}(s)^{(ij)} = \sum_{n=1}^d \mathbf{w}_2^{(in)} \cdot \mathbf{w}_1^{(nj)} \quad (13)$$

and the probability of an element in the sum chain  $\sum_{n=1}^d \mathbf{w}_2^{(in)} \cdot \mathbf{w}_1^{(nj)}$  being dense is upper bounded as:

$$Pr \left( \mathbf{w}_2^{(in)} \cdot \mathbf{w}_1^{(nj)} \neq 0 \right) \leq \frac{k_{\mathbf{w}_2}^{(i)} k_{\mathbf{w}_1}^{(j)}}{d^2}, \quad (14)$$

As long as there is an element in the sum chain is non-zero, the entry of gradient is non-zero. So, from here we can quantify the bound of the probability of input gradient entry  $\nabla_{s[t]} p_{\mathbf{w}}(s)^{(ij)}$  being dense as:

$$Pr \left( \nabla_{s[t]} p_{\mathbf{w}}(s)^{(ij)} \neq 0 \right) \leq \frac{k_{\mathbf{w}_2}^{(i)} k_{\mathbf{w}_1}^{(j)}}{d^2}, \quad (15)$$

and the expectation of the input gradient  $L_0$  norm across  $d \times d$  matrix is:

$$\mathbb{E} [\| \nabla_{s[t]} p_{\mathbf{w}}(s) \|_0] \leq k_{\mathbf{w}_2}^{(i)} k_{\mathbf{w}_1}^{(j)} \quad (16)$$

Similar derivation process can be applied to the  $\mathbf{w}_1$  weight gradient and obtain its  $L_0$  expectation. We start with an element of the sum chain  $\sum_{n=1}^d \mathbf{w}_2^{(in)} \cdot S^{(nj)}$  as:

$$Pr \left( \mathbf{w}_2^{(in)} \cdot S^{(nj)} \neq 0 \right) \leq \frac{k_{\mathbf{w}_2}^{(i)} k_S^{(j)}}{d^2} \Leftrightarrow \mathbb{E} [\| \nabla_{\mathbf{w}_1} p_{\mathbf{w}}(s) \|_0] \leq T \cdot \frac{k_{\mathbf{w}_2}^{(i)} k_S^{(j)}}{d} \quad (17)$$

Divide obtained inequalities from Equation 16 and 17:

$$\begin{aligned} \frac{\mathbb{E} [\| \nabla_{\mathbf{w}_1} p_{\mathbf{w}}(s) \|_0]}{\mathbb{E} [\| \nabla_{s[t]} p_{\mathbf{w}}(s) \|_0]} &\leq \frac{T \cdot \frac{k_{\mathbf{w}_2}^{(i)} k_S^{(j)}}{d}}{\frac{k_{\mathbf{w}_2}^{(i)} k_{\mathbf{w}_1}^{(j)}}{d}} \\ \Leftrightarrow \mathbb{E} [\| \nabla_{\mathbf{w}_1} p_{\mathbf{w}}(s) \|_0] &\leq \frac{T}{d} \cdot \frac{k_{\mathbf{w}_2}^{(i)} k_S^{(j)}}{k_{\mathbf{w}_2}^{(i)} k_{\mathbf{w}_1}^{(j)}} \cdot \mathbb{E} [\| \nabla_{s[t]} p_{\mathbf{w}}(s) \|_0]. \\ \Leftrightarrow \mathbb{E} [\| \nabla_{\mathbf{w}_1} p_{\mathbf{w}}(s) \|_0] &\leq \frac{T}{d} \cdot \frac{k_S^{(j)}}{k_{\mathbf{w}_1}^{(j)}} \cdot \mathbb{E} [\| \nabla_{s[t]} p_{\mathbf{w}}(s) \|_0]. \end{aligned} \quad (18)$$

As observed from derivation results, weight gradient density is bounded by input gradient density by a factor of  $\frac{T}{d} \cdot \frac{k_S^{(j)}}{k_{\mathbf{w}_1}^{(j)}}$ .  $\square$

## 6 LIMITATIONS AND FUTURE WORKS

While our study presents strong evidence linking gradient density-sparsity to adversarial robustness-generalization trade off in SNNs, an all-rounded method for proper generalization-adversarial robustness improvement was not proposed.

Still, this lead to several open avenues for exploration such as sparsity-aware architecture design where future architectures could be explicitly designed to balance natural and architectural sparsity, creating an optimal trade-offs between robustness and accuracy. This may involve hybrid pooling mechanisms or novel spike-based normalization layers that retain desirable sparsity characteristics. Optionally, we can also focus on a more effective attack methods on SNN models, targeting those with very sparse gradient causing white-box gradient based attacks to be ineffective.

## 7 CONCLUSION

In this work, we systematically evaluated the trade off between adversarial robustness and generalization of undefended SNNs. Through benchmarking various datasets, we observed that these models demonstrate competitive robustness against traditional white-box attacks, often surpassing

existing SOTA defense mechanisms without any explicit adversarial training or defense augmentation. To investigate the root cause of this behavior, we empirically validated this relationship by analyzing the input gradient distributions of SNN, revealing substantial gradient sparsity across various operations. We further categorized this sparsity into *architectural sparsity*, arising from structural components and *natural sparsity*, which is intrinsic to the spiking nature of SNNs. Our experiments led to a measurable reduction in gradient sparsity and a corresponding decrease in adversarial robustness, confirming the trade-off between robustness and generalization.

## DATA AVAILABILITY

Source code is publicly available at <https://github.com/luutn2002/grad-obf-snn>.

## REFERENCES

Krizhevsky Alex. Learning multiple layers of features from tiny images. *https://www.cs.toronto.edu/kriz/learning-features-2009-TR.pdf*, 2009.

Anish Athalye, Nicholas Carlini, and David Wagner. Obfuscated gradients give a false sense of security: Circumventing defenses to adversarial examples. In *International conference on machine learning*, pp. 274–283. PMLR, 2018a.

Anish Athalye, Logan Engstrom, Andrew Ilyas, and Kevin Kwok. Synthesizing robust adversarial examples. In *International conference on machine learning*, pp. 284–293. PMLR, 2018b.

Daniel Auge, Julian Hille, Etienne Mueller, and Alois Knoll. A survey of encoding techniques for signal processing in spiking neural networks. *Neural Processing Letters*, 53(6):4693–4710, 2021.

David Baehrens, Timon Schroeter, Stefan Harmeling, Motoaki Kawanabe, Katja Hansen, and Klaus-Robert Müller. How to explain individual classification decisions. *The Journal of Machine Learning Research*, 11:1803–1831, 2010.

Peter Blouw, Xuan Choo, Eric Hunsberger, and Chris Eliasmith. Benchmarking keyword spotting efficiency on neuromorphic hardware. In *Proceedings of the 7th annual neuro-inspired computational elements workshop*, pp. 1–8, 2019.

Rich Caruana, Yin Lou, Johannes Gehrke, Paul Koch, Marc Sturm, and Noemie Elhadad. Inelligible models for healthcare: Predicting pneumonia risk and hospital 30-day readmission. In *Proceedings of the 21th ACM SIGKDD International Conference on Knowledge Discovery and Data Mining*, KDD ’15, pp. 1721–1730, New York, NY, USA, 2015. Association for Computing Machinery. ISBN 9781450336642. doi: 10.1145/2783258.2788613. URL <https://doi.org/10.1145/2783258.2788613>.

Jianhao Ding, Tong Bu, Zhaofei Yu, Tiejun Huang, and Jian Liu. Snn-rat: Robustness-enhanced spiking neural network through regularized adversarial training. *Advances in Neural Information Processing Systems*, 35:24780–24793, 2022.

Jason K Eshraghian, Max Ward, Emre O Neftci, Xinxin Wang, Gregor Lenz, Girish Dwivedi, Mohammed Bennamoun, Doo Seok Jeong, and Wei D Lu. Training spiking neural networks using lessons from deep learning. *Proceedings of the IEEE*, 2023.

Steve K Esser, Rathinakumar Appuswamy, Paul Merolla, John V Arthur, and Dharmendra S Modha. Backpropagation for energy-efficient neuromorphic computing. *Advances in neural information processing systems*, 28, 2015.

Wei Fang, Zhaofei Yu, Yanqi Chen, Tiejun Huang, Timothée Masquelier, and Yonghong Tian. Deep residual learning in spiking neural networks. *Advances in Neural Information Processing Systems*, 34:21056–21069, 2021a.

Wei Fang, Zhaofei Yu, Yanqi Chen, Timothée Masquelier, Tiejun Huang, and Yonghong Tian. Incorporating learnable membrane time constant to enhance learning of spiking neural networks. In *Proceedings of the IEEE/CVF international conference on computer vision*, pp. 2661–2671, 2021b.

Wei Fang, Yanqi Chen, Jianhao Ding, Zhaofei Yu, Timothée Masquelier, Ding Chen, Liwei Huang, Huihui Zhou, Guoqi Li, and Yonghong Tian. Spikingjelly: An open-source machine learning infrastructure platform for spike-based intelligence. *Science Advances*, 9(40):eadi1480, 2023. doi: 10.1126/sciadv.adi1480. URL <https://www.science.org/doi/abs/10.1126/sciadv.adi1480>.

Anthony W Flores, Kristin Bechtel, and Christopher T Lowenkamp. False positives, false negatives, and false analyses: A rejoinder to machine bias: There's software used across the country to predict future criminals. and it's biased against blacks. *Fed. Probation*, 80:38, 2016.

Wulfram Gerstner and Werner M Kistler. *Spiking neuron models: Single neurons, populations, plasticity*. Cambridge university press, 2002.

Ian J Goodfellow, Jonathon Shlens, and Christian Szegedy. Explaining and harnessing adversarial examples. *arXiv preprint arXiv:1412.6572*, 2014.

Yangfan Hu, Huajin Tang, and Gang Pan. Spiking deep residual networks. *IEEE Transactions on Neural Networks and Learning Systems*, 34(8):5200–5205, 2021.

Jaehyun Kim, Heesu Kim, Subin Huh, Jinho Lee, and Kiyoung Choi. Deep neural networks with weighted spikes. *Neurocomputing*, 311:373–386, 2018.

Diederik P Kingma and Jimmy Ba. Adam: A method for stochastic optimization. *arXiv preprint arXiv:1412.6980*, 2014.

Souvik Kundu, Massoud Pedram, and Peter A Beerel. Hire-snn: Harnessing the inherent robustness of energy-efficient deep spiking neural networks by training with crafted input noise. In *Proceedings of the IEEE/CVF international conference on computer vision*, pp. 5209–5218, 2021.

Alexey Kurakin, Ian Goodfellow, and Samy Bengio. Adversarial machine learning at scale. *arXiv preprint arXiv:1611.01236*, 2016.

Alexey Kurakin, Ian J Goodfellow, and Samy Bengio. Adversarial examples in the physical world. In *Artificial intelligence safety and security*, pp. 99–112. Chapman and Hall/CRC, 2018.

Chankyu Lee, Priyadarshini Panda, Gopalakrishnan Srinivasan, and Kaushik Roy. Training deep spiking convolutional neural networks with stdp-based unsupervised pre-training followed by supervised fine-tuning. *Frontiers in neuroscience*, 12:435, 2018.

Chankyu Lee, Syed Shakib Sarwar, Priyadarshini Panda, Gopalakrishnan Srinivasan, and Kaushik Roy. Enabling spike-based backpropagation for training deep neural network architectures. *Frontiers in neuroscience*, 14:497482, 2020.

Fangxin Liu, Wenbo Zhao, Yongbiao Chen, Zongwu Wang, Tao Yang, and Li Jiang. Sstdp: Supervised spike timing dependent plasticity for efficient spiking neural network training. *Frontiers in Neuroscience*, 15:756876, 2021.

Yujia Liu, Tong Bu, Jianhao Ding, Zecheng Hao, Tiejun Huang, and Zhaofei Yu. Enhancing adversarial robustness in snns with sparse gradients. *arXiv preprint arXiv:2405.20355*, 2024.

Nhan Luu, Duong Luu, Pham Ngoc Nam, and Truong Cong Thang. Improvement of spiking neural network with bit plane coding. In *2024 IEEE 16th International Conference on Computational Intelligence and Communication Networks (CICN)*. IEEE, 2024a.

Nhan T Luu, Chibuike Onuoha, and Truong Cong Thang. Blind image quality assessment with multimodal prompt learning. In *2023 IEEE 15th International Conference on Computational Intelligence and Communication Networks (CICN)*, pp. 614–618. IEEE, 2023.

Nhan T Luu, Duong T Luu, Nam N Pham, and Thang C Truong. Improvement of spiking neural network with bit planes and color models. *arXiv preprint arXiv:2410.08229*, 2024b.

Nhan T Luu, Thang C Truong, and Duong T Luu. Universal quantum tomography with deep neural networks. *arXiv preprint arXiv:2407.01734*, 2024c.

Wolfgang Maass. Networks of spiking neurons: the third generation of neural network models. *Neural networks*, 10(9):1659–1671, 1997.

Aleksander Madry, Aleksandar Makelov, Ludwig Schmidt, Dimitris Tsipras, and Adrian Vladu. Towards deep learning models resistant to adversarial attacks. *arXiv preprint arXiv:1706.06083*, 2017.

Paul A Merolla, John V Arthur, Rodrigo Alvarez-Icaza, Andrew S Cassidy, Jun Sawada, Philipp Akopyan, Bryan L Jackson, Nabil Imam, Chen Guo, Yutaka Nakamura, et al. A million spiking-neuron integrated circuit with a scalable communication network and interface. *Science*, 345(6197):668–673, 2014.

Emre O Neftci, Hesham Mostafa, and Friedemann Zenke. Surrogate gradient learning in spiking neural networks: Bringing the power of gradient-based optimization to spiking neural networks. *IEEE Signal Processing Magazine*, 36(6):51–63, 2019.

Duy-Anh Nguyen, Xuan-Tu Tran, and Francesca Iacopi. A review of algorithms and hardware implementations for spiking neural networks. *Journal of Low Power Electronics and Applications*, 11(2):23, 2021.

Joao D Nunes, Marcelo Carvalho, Diogo Carneiro, and Jaime S Cardoso. Spiking neural networks: A survey. *IEEE Access*, 10:60738–60764, 2022.

Nicolas Papernot, Patrick McDaniel, Ian Goodfellow, Somesh Jha, Z Berkay Celik, and Ananthram Swami. Practical black-box attacks against machine learning. In *Proceedings of the 2017 ACM on Asia conference on computer and communications security*, pp. 506–519, 2017.

Adam Paszke, Sam Gross, Francisco Massa, Adam Lerer, James Bradbury, Gregory Chanan, Trevor Killeen, Zeming Lin, Natalia Gimelshein, Luca Antiga, et al. Pytorch: An imperative style, high-performance deep learning library. *Advances in neural information processing systems*, 32, 2019.

David Picard. Torch. manual\_seed (3407) is all you need: On the influence of random seeds in deep learning architectures for computer vision. *arXiv preprint arXiv:2109.08203*, 2021.

Bipin Rajendran, Abu Sebastian, Michael Schmuker, Narayan Srinivasa, and Evangelos Eleftheriou. Low-power neuromorphic hardware for signal processing applications: A review of architectural and system-level design approaches. *IEEE Signal Processing Magazine*, 36(6):97–110, 2019.

Marco Tulio Ribeiro, Sameer Singh, and Carlos Guestrin. ” why should i trust you?” explaining the predictions of any classifier. In *Proceedings of the 22nd ACM SIGKDD international conference on knowledge discovery and data mining*, pp. 1135–1144, 2016.

Andrew Ross and Finale Doshi-Velez. Improving the adversarial robustness and interpretability of deep neural networks by regularizing their input gradients. In *Proceedings of the AAAI conference on artificial intelligence*, volume 32, 2018.

Bodo Rueckauer, Iulia-Alexandra Lungu, Yuhuang Hu, Michael Pfeiffer, and Shih-Chii Liu. Conversion of continuous-valued deep networks to efficient event-driven networks for image classification. *Frontiers in neuroscience*, 11:682, 2017.

David E Rumelhart, Geoffrey E Hinton, and Ronald J Williams. Learning representations by back-propagating errors. *nature*, 323(6088):533–536, 1986.

Shai Shalev-Shwartz, Ohad Shamir, and Shaked Shammah. Failures of gradient-based deep learning. In *International Conference on Machine Learning*, pp. 3067–3075. PMLR, 2017.

Saima Sharmin, Nitin Rathi, Priyadarshini Panda, and Kaushik Roy. Inherent adversarial robustness of deep spiking neural networks: Effects of discrete input encoding and non-linear activations. In *European Conference on Computer Vision*, pp. 399–414. Springer, 2020.

Sumit B Shrestha and Garrick Orchard. Slayer: Spike layer error reassignment in time. *Advances in neural information processing systems*, 31, 2018.

Daniel Smilkov, Nikhil Thorat, Been Kim, Fernanda Viégas, and Martin Wattenberg. Smoothgrad: removing noise by adding noise. *arXiv preprint arXiv:1706.03825*, 2017.

Gopalakrishnan Srinivasan, Sourya Roy, Vijay Raghunathan, and Kaushik Roy. Spike timing dependent plasticity based enhanced self-learning for efficient pattern recognition in spiking neural networks. In *2017 International Joint Conference on Neural Networks (IJCNN)*, pp. 1847–1854. IEEE, 2017.

Mukund Sundararajan, Ankur Taly, and Qiqi Yan. Gradients of counterfactuals. *arXiv preprint arXiv:1611.02639*, 2016.

Christian Szegedy, Wojciech Zaremba, Ilya Sutskever, Joan Bruna, Dumitru Erhan, Ian Goodfellow, and Rob Fergus. Intriguing properties of neural networks. *arXiv preprint arXiv:1312.6199*, 2013.

Florian Tramèr, Alexey Kurakin, Nicolas Papernot, Ian Goodfellow, Dan Boneh, and Patrick McDaniel. Ensemble adversarial training: Attacks and defenses. *arXiv preprint arXiv:1705.07204*, 2017a.

Florian Tramèr, Nicolas Papernot, Ian Goodfellow, Dan Boneh, and Patrick McDaniel. The space of transferable adversarial examples. *arXiv preprint arXiv:1704.03453*, 2017b.

Jason Wang, Luis Perez, et al. The effectiveness of data augmentation in image classification using deep learning. *Convolutional Neural Networks Vis. Recognit*, 11(2017):1–8, 2017.

M Arif Wani, Farooq Ahmad Bhat, Saduf Afzal, and Asif Iqbal Khan. *Advances in deep learning*. Springer, 2020.

Weilin Xu, David Evans, and Yanjun Qi. Feature squeezing: Detecting adversarial examples in deep neural networks. *arXiv preprint arXiv:1704.01155*, 2017.

Friedemann Zenke and Surya Ganguli. Superspike: Supervised learning in multilayer spiking neural networks. *Neural computation*, 30(6):1514–1541, 2018.

Friedemann Zenke and Tim P Vogels. The remarkable robustness of surrogate gradient learning for instilling complex function in spiking neural networks. *Neural computation*, 33(4):899–925, 2021.